MMLPA: Multilayered Metamaterial Low Profile Antenna for IoT Applications

A Thesis Submitted to the Department of Computer Science and Communications Engineering, the Graduate School of Fundamental Science and Engineering of Waseda University in Partial Fulfillment of the Requirements for the Degree of Master of Engineering

July 24th, 2018

Tojoarisoa Rakotoaritina

(5116FG26-9)

Advisor: Prof. Shigeru Shimamoto

Research guidance: Research on Wireless Access

Acknowledgement

This thesis summarizes the achievements of my research in Graduate School of Fundamental Science and Engineering, Department of Computer Science and Communications Engineering, Waseda University, Japan.

I thank God for bringing me to Japan and giving me the wisdom and the strength to accomplish my studies.

I would like to express my great acknowledgement to my supervisor, Prof. Shigeru Shimamoto, for his invaluable guidance, contributions, and suggestions that helped me complete this thesis.

I would like to express my gratitude to all the members in Shimamoto Laboratory, especially, Dr. Jiang Liu, Dr. Zhenni Pan, Ms. Megumi Saito for their support and technical discussions.

In addition, special thanks also to all faculty members, staff, and friends in Waseda University.

I am very proud of being awarded the ABE initiative scholarship from Japanese Government. I would like to express my gratitude to JICA for the financial support. I also received generous support from JICE. I am particularly grateful for the assistance given by Ms. Asano Kumiko.

Last but not least, I have been blessed with the most wonderful and supportive family any one can wish for. There is little I can say to thank you all. I thank God for the support, love, and devotion of my wife Henintsoa Rambinimasina as well.

Tojoarisoa RAKOTOARITINA

July 2018

Abstract

Nowadays, within the concept of Internet of Things (IoT), smart homes, smart factory, intelligent transportation, smart agriculture networks among others, are infrastructure systems that connect our world to the Internet. However, wireless communications technology, such as wireless cellular networks, wireless area networks, wireless sensor networks, and vehicular communications among others, are considerably constrained by complicated structures, and lossy media in complex environments. Fundamental limitations on the transmission range have been treated to connect IoT devices in complex environments. In order to extend the transmission range in complex environments, Magnetic Induction (MI) communication has been proved to be an efficient solution. In this thesis, Multilayered Metamaterial Low Profile Antennas (MMLPA) using Magnetic Induction communication scheme are designed and prototyped for IoT applications. The channel model of the MMLPA system is analyzed. Then four models of MMLPA system are designed by using circular loop antennas backed with isotropic metamaterial which is considered as Defected Ground Structure (DGS) as well as with anisotropic metamaterial for the purpose of dielectric uniaxial metamaterial. To the best of our knowledge, this is the first work that investigates the performance of a magnetic loop antenna coil backed with multiple layers of isotropic and anisotropic metamaterials for IoT applications in environment that are hostile, RF challenged, and especially in the vicinity of metal. By using a full-wave finite-element method, the proposed analysis is supported with simulation results where good agreement is achieved compared to the measurement results after realizing four prototypes of the MMLPA antennas. The effect of the presence of metal in the vicinity of the transceivers is also analyzed. A MMLPA-IoT system is developed for IoT applications.

Keywords—IoT; MI communication; M^2I; MMLPA; MMLPA-IoT; near metal environments; RF challenging environments.

Table of Contents

List of Figures

Chapter 1

Introduction

1.1 Background

The IoT provides many new opportunities to the end user and the industry in many applications fields. Currently, however, the IoT itself lacks theory, technology architecture, and standards that integrate the virtual world and the real physical world in a unified framework [1]. According to [2], the IoT should have three characteristics: (1) comprehensive perception, (2) reliable transmission, (3) intelligent processing. However, in wireless communications technology, such as wireless cellular networks, wireless area networks, wireless sensor networks, and vehicular communications among others, are considerably constrained by complicated structures, and lossy media in complex environments. Magnetic Induction (MI) communication has been proved to be an efficient solution to extend the communication range in such environments, like underground [3], underwater [4], and in the vicinity of metal. Therefore, within the wider context of IoT, MI communication has attracted significant research interests in recent years.

Magnetic Induction belongs to the wireless communication technology especially in the RF challenging environment. The basic MI communication system uses magnetic antenna coils for transmitting and receiving information as well as power, and it has been commonly used in near field communication. Since the propagation medium is soil, water, air with presence or absence of metal in the vicinity of the transceivers, wireless signal experience high absorption and multiple scattering due to which path loss increases, as a result the transmission range is extremely short. To this end, existing terrestrial wireless communication techniques have to use large antennas and high transmission power which are not convenient and not efficient. Magnetic induction solves this problem by using small size antennas in underground [3] and underwater [4].

MI system utilizes a high frequency magnetic field which is generated by a transmitter coil as a signal carrier [5]. It mostly depends on the permeability of the communication medium.

The performance of MI communication remains same in most materials, since most natural materials have the same magnetic permeability as air. This guarantees the fact that this wireless technology also solves the dynamic channel condition issue.

Despite these benefits, one drawback with MI communication scheme is fast attenuation of magnetic field which mainly causes the short transmission range. To solve this problem, different methods have been used such as waveguide structures [6], metamaterial enhanced Magnetic Induction communication [7], etc. Metamaterial is defined as a composite material with a specific structure such that it exhibits properties, not usually found in natural materials, such as negative permeability ($\mu = -1$) or negative permittivity ($\varepsilon = -1$). These properties of the metamaterial can affect the electromagnetic waves. It is important to note that metamaterial has been utilized in antenna miniaturization [8] and wireless power transfer [9] which are the two most relevant areas related to MI communication.

1.2 Thesis objectives

In this thesis, we propose Multilayered Metamaterial Low Profile Antenna using Magnetic Induction (MMLPA) communication scheme by designing MMLPA antennas with high directivity in order to increase the communication range for IoT applications in environment that are hostile, RF challenged, and especially in the vicinity of metal.

In this scheme, MI antenna coils are composed with n layers of isotropic and anisotropic metamaterials. For computation time complexity reason, one metamaterial shell composed with one layer of isotropic metamaterial and another layer of anisotropic metamaterial were chosen for the simulation as shown in Fig.1. The results in [10] show that the absorption of the electromagnetic wave is about 100% near the resonant frequency of the isotropic metamaterials. In addition, the anisotropic metamaterials can be used to be the polarization tunable absorber. Therefore, combining these two kinds of metamaterials will be beneficial for the directivity and efficiency of the MMLPA system. The equivalent circuit model for MMLPA is given and the general path loss formula is also derived. Ansys HFSS v15.0 is used for the designing and simulation of MMLPA system.

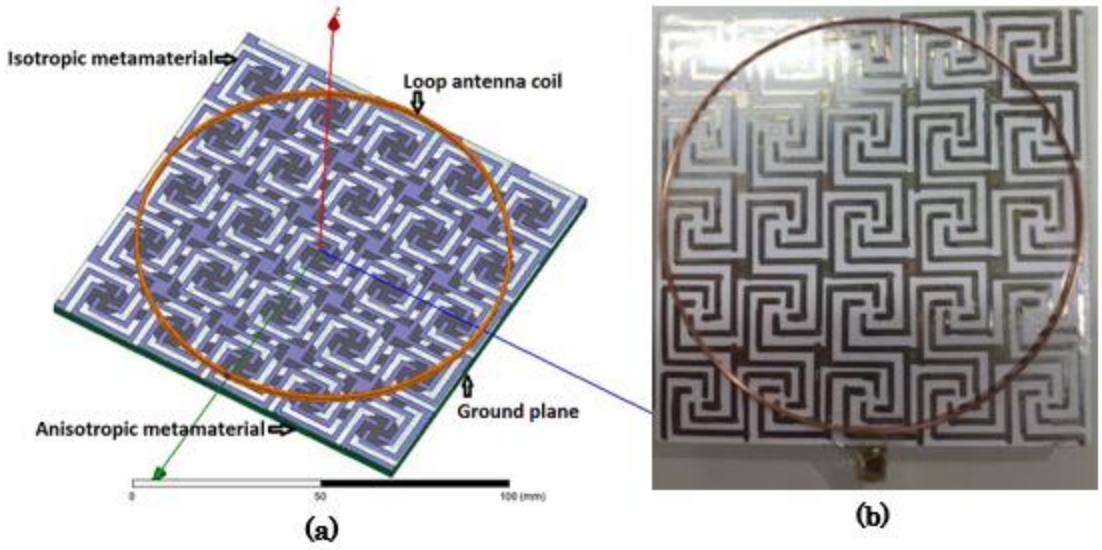

Fig. 1. MMLPA system: (a) the designed antenna, (b) the prototyped antenna

1.3 Thesis organization

This thesis is organized as follows:

In chapter 2, the literature review is described including related works.

Then, the system model is developed in chapter 3 which includes an analytical channel model for MMLPA wireless system as well as derivation of the communication range and definition of the S parameters.

In chapter 4, design procedure is presented including the design of the MMLPA system, the details of the simulation procedure as well.

The simulation and experimental results are discussed in chapter 5.

After that, an IoT application is developed in chapter 6.

Finally, this thesis is concluded in Chapter 7.

Chapter 2

Literature Review

MI communication scheme has been utilized in various complex environments. In underground mines, voice and low data rate communications have been established by using MI scheme [11]. In [5], very large MI coil antennas have been utilized in underwater environment. MI has been utilized to transmit both data and power into human body for medical applications as well [12]. In [13], MI waveguides structures have been utilized to extend the very limited transmission range. However, these waveguides require very high density of relay coils which prevents practical implementation.

Metamaterial has also been utilized in many applications. For instance, metamaterial antenna [9], Metamaterial enhanced magnetic induction Antenna for Magnetic Resonance Imaging [14], and metamaterial cloak. Our work is mainly focused on two areas which are antenna miniaturization and wireless power transfer among various research related to metamaterial. In [15], metamaterial has been utilized in antenna miniaturization. As shown in [16], the radiated power is dramatically amplified when the electrical dipole antenna is enclosed in a metamaterial shell. It is also shown in [10] that metamaterial slab between two resonant coils can enhance the near field coupling. In [17], the power transfer efficiency can be greater in magnitude than the free space efficiency with the slab. The metamaterial volume between the coils can be compressed by using magnetic permeability having large anisotropy ratio.

In [18], metamaterial is also utilized to enhance the magnetic field around MI transceivers, and this is done by enclosing the antenna coil by a metamaterial shell which amplifies the magnetic field both at transmitter side and receiver side. As a result, the system can achieve increased transmission range. The scheme proposed in this thesis basically focuses on increasing the magnetic field around MI transceivers by considering multiple layers of metamaterial shell while keeping the size of the antennas small.

Chapter 3

System model

3.1 Derivation of the communication range

The analytical channel model of MMLPA is developed in this section. In MMLPA system as illustrated in Fig.1, the performance of MI communication using loop antenna coil can be enhanced when it is backed with n layers of metamaterials. The number of metamaterial layers can be set as well as its thickness while keeping the size of the antenna small and making it low profile. According to previous work in [7], an equivalent circuit can be modelled for the channel. The equivalent circuit of MMLPA system is modelled as shown in Fig.2.

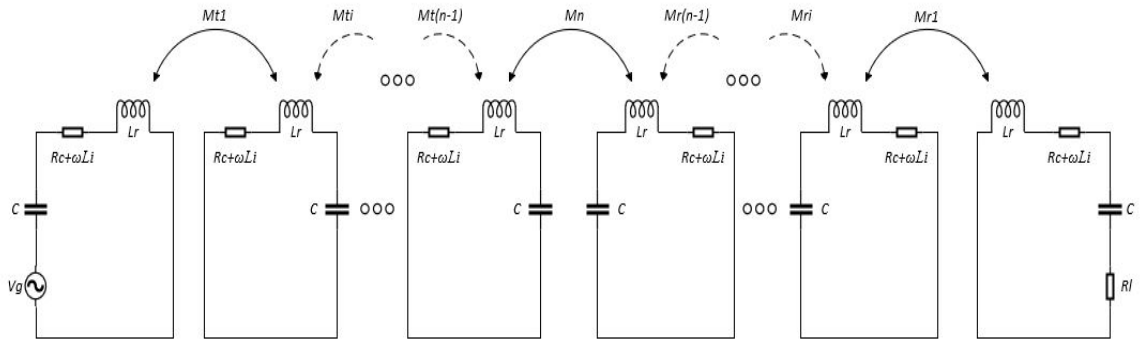

Fig. 2. Equivalent circuit model of MMLPA communication

Where: Vg is the source voltage; Rc is the resistance of the coil; Lr is the self-inductance of the coil; C is the compensation capacitor which is used to tune the circuit at resonant; Mn is the mutual inductance between MMLPA transmitter and MMLPA receiver. Mt1, …, Mt(n-1) are the mutual inductance between the transmitter coil enclosed by the first metamaterial shell and the second metamaterial shell at the transmitter side, …, the mutual inductance between the (n-1)-th metamaterial shell and the n-th metamaterial shell at the transmitter side respectively. Similarly, Mr1, …, Mr(n-1) are the mutual inductance between the receiver coil enclosed by the first metamaterial shell and the second metamaterial shell at the receiver side, …, the mutual inductance between the (n-1)-th

metamaterial shell and the n-th metamaterial shell at the receiver side respectively; Rl is the load resistance.

In order to achieve the resonance condition for the circuit, the compensation capacitor C is given by:

$$C = \frac{1}{\omega_0^2 Lr} \tag{1}$$

where ω_0 is the resonant frequency of the coil. According to [7], the self-inductance L becomes frequency dependent complex number:

$$L = Lr - jLi \tag{2}$$

where the imaginary part Li becomes frequency dependent resistance which is due to the induced eddy current from the metamaterial layers and the complex environment. Therefore, the real part Lr is the self-inductance of the coil and once the reactance at transmitter and receiver are cancelled, the load resistance of the coil at the receiver side is matched with the resistance of the coil Rc and additional loss ωLi.

Based on the equivalent circuit represented in Fig.2., the path loss for MMLPA channel, which is the main factor that decides the transmission range, can be expressed as:

$$PL = -10\log\left\{\frac{\mathrm{Pr}}{Pt}\right\} \tag{3}$$

where Pt and Pr are the transmitted and received power respectively. We have:

$$\frac{\Pr}{Pt}=\frac{\begin{array}{l}\left(\omega^2\right)^{2n-1}\left|Mn\right|^2\prod_{k=1}^{n-1}\left|Mtk\right|^2\left|Mrk\right|^2\dfrac{Rl}{\left(Rc+\omega Li\right)^2\left(Rc+Rl+\omega Li\right)}\\ -\omega^2\left|Mn\right|^2\left(Rc+Rl+\omega Li\right)\\ +\omega^2\prod_{k=1}^{n-1}\left|Mrk\right|^2\left(Rc+\omega Li\right)\end{array}}{\begin{array}{l}\left(Rc+\omega Li\right)^{2n-1}\left(Rc+Rl+\omega Li\right)\\ -\omega^2\left|Mn\right|^2\left(Rc+\omega Li\right)\left(Rc+Rl+\omega Li\right)\\ +\omega^{2n}\prod_{k=1}^{n-1}\left|Mtk\right|^2\left|Mrk\right|^2\\ +\omega^2\sum_{k=1}^{n-1}\left|Mtk\right|^2\left(Rc+\omega Li\right)\left(Rc+Rl+\omega Li\right)\\ +\omega^2\sum_{k=1}^{n-1}\left|Mrk\right|^2\left(Rc+\omega Li\right)^2\end{array}} \quad (4)$$

Assume that Mtk = Mrk = Mn = M for k=1,…, n-1; therefore:

$$\frac{\Pr}{Pt}=\frac{\begin{array}{l}\left(\omega^2\left|M\right|^2\right)^{2n-1}\dfrac{Rl}{\left(Rc+\omega Li\right)^2\left(Rc+Rl+\omega Li\right)}\\ -\omega^2\left|M\right|^2\left(Rc+Rl+\omega Li\right)\\ +\omega^2\left(\left|M\right|^2\right)^{n-1}\left(Rc+\omega Li\right)\end{array}}{\begin{array}{l}\left(Rc+\omega Li\right)^{2n-1}\left(Rc+Rl+\omega Li\right)\\ -\omega^2\left|M\right|^2\left(Rc+\omega Li\right)\left(Rc+Rl+\omega Li\right)\\ +\omega^{2n}\left(\left|M\right|^2\right)^{2n-2}\\ +\left(n-1\right)\omega^2\left|M\right|^2\left(Rc+\omega Li\right)\left(Rc+Rl+\omega Li\right)\\ +\left(n-1\right)\omega^2\left|M\right|^2\left(Rc+\omega Li\right)^2\end{array}} \quad (5)$$

$$\frac{\Pr}{\mathrm{P}t}\approx\frac{\left(\omega^2\left|M\right|^2\right)^{2n-1}}{\left(\left(Rc+\omega Li\right)^2\right)^{2n-1}} \quad (6)$$

Then, the path loss is derived as below:

$$PL\approx -20\left(2n-1\right)\log\left(\frac{\omega\left|M\right|}{\left(Rc+\omega Li\right)}\right) \quad (7)$$

In this thesis, since air is considered as the transmission medium with presence or absence of metal in the vicinity of the MMLPA transceivers, the derivation of the communication range can be seen below according to the Friis transmission equation:

$$\frac{\mathrm{Pr}}{Pt} = \frac{GtGr\lambda^2}{\left(4\pi d\right)^2} \tag{8}$$

Where: Gt and Gr are the gain of the transmitting and receiving antenna respectively, λ is the wavelength, and d is the distance between the transmitter and the receiver antennas.

Therefore, according to (6):

$$\frac{GtGrc^2}{\left(2\pi d\omega\right)^2} = \frac{\left(\omega^2 |M|^2\right)^{2n-1}}{\left(\left(Rc+\omega Li\right)^2\right)^{2n-1}} \tag{9}$$

Where: c is the velocity of the light and $\omega = 2\pi f$ is the angular frequency.

Consequently, the communication range is derived as below:

$$d = \frac{c\sqrt{GtGr}}{2\pi\omega}\left(\frac{Rc+\omega Li}{\omega|M|}\right)^{2n-1} \tag{10}$$

From this expression, we can confirm that the communication range is also proportional to the gain of the transmitting and receiving antennas.

The developed channel model reveals that both the MMLPA coil antenna and the propagation channel are susceptible to frequency change. On one hand, the low frequency band is almost immune to high conductivity due to the long wavelength, while high frequency band has very small skin depth in complex environments which leads to significant loss. On the other hand, motivated by the fact that high frequency can provide strong coupling between MMLPA coil antennas as well as broader bandwidth which are essential for wireless communication, air with presence or absence of metal in the vicinity of the MMLPA system transceivers is considered as the propagation medium along this work.

It is also important to note that there is a tradeoff between efficiency, antenna size and medium conductivity. To overcome the high absorption loss in large complex environments, relatively low frequency is utilized. However, this requires a large profile antenna to achieve high efficiency. When conductivity is small, magnetic fields have similar intensity. However, when the conductivity becomes large, the magnetic fields intensity of lower frequency is much larger than that of higher frequency. Therefore, with similar field intensity, high frequency can provide much larger bandwidth which is favorable for our wireless communication system.

Consequently, the optimal frequency for MMLPA communication is highly influenced by the medium conductivity, the antenna size and the frequency ranges from low frequency to high frequency band.

3.2 Definition of the S parameters of a normally incident plane wave on a metamaterial cube

Consider a normally incident plane wave on the metamaterial cube shown in Fig.3. below.

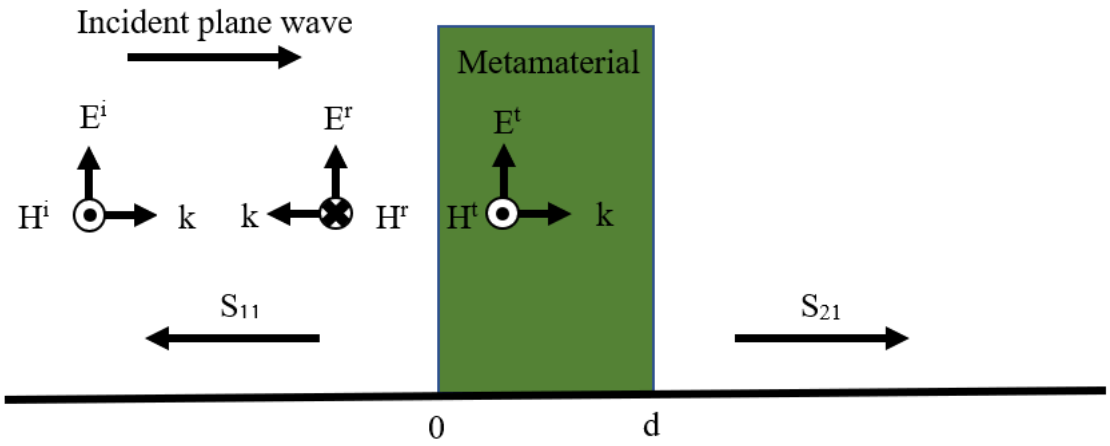

Fig. 3. A normally incident plane wave on a metamaterial placed in free space

According to [15], the S parameters of this system can be derived as:

$$S_{11} = \frac{R_{01}\left(1-e^{i2refk_0d}\right)}{1-R_{01}^2 e^{i2refk_0d}} \qquad (11)$$

$$S_{21} = \frac{(1-R_{01}^2)e^{i2refk_0d}}{1-R_{01}^2e^{i2refk_0d}} \quad (12)$$

The impedance z, which is the solution of equations (11) and (12), is written as:

$$z = \pm\sqrt{\frac{(1+S_{11})^2 - S_{21}^2}{(1-S_{11})^2 - S_{21}^2}} \quad (13)$$

$$e^{irefk_0d} = \frac{S_{21}}{1-S_{11}\dfrac{z-1}{z+1}} \quad (14)$$

$$ref = \frac{1}{k_0d}\left\{\left(\left(\ln\left(e^{irefk_0d}\right)\right)'' + 2m\pi\right) - i\left(\ln\left(e^{irefk_0d}\right)\right)'\right\} \quad (15)$$

Where: S_{11} and S_{21} are the reflection and transmission coefficients respectively, R_{01} is $\dfrac{z-1}{z+1}$, ref is the refractive index, k_0 is the wave number, d is the maximum length of the unit element of the metamaterial, m is the branch due to the periodicity of the sinusoidal function, E and H are the electric and magnetic field components respectively, $(\bullet)^i$, $(\bullet)^r$ and $(\bullet)^t$ are the incident, reflected and transmitted components of the fields respectively, $(\bullet)'$ and $(\bullet)''$ represent the real and complex components of the complex number.

It is important to note that, in theses expressions, the metamaterial is represented by the cube formed by the unit element with appropriate boundary conditions and excitations.

In this thesis, the metamaterial is assumed to be homogeneous with an effective refractive index and impedance. According to [16], we can choose the fundamental branch ($m = 0$) for a continuous refractive index and consider that the largest dimension of the metamaterial unit cell is less than one-sixth of wavelength in the material.

Chapter 4

Design procedure

4.1 MMLPA system design

The MMLPA system is designed using circular loop antenna coil backed with different layers of isotropic and anisotropic metamaterials.

4.1.1 Loop antenna:

The coil antenna is made by copper wire with: inner diameter 100 mm, outer diameter 101.6 mm, thickness 2.13 mm and 52 turns.

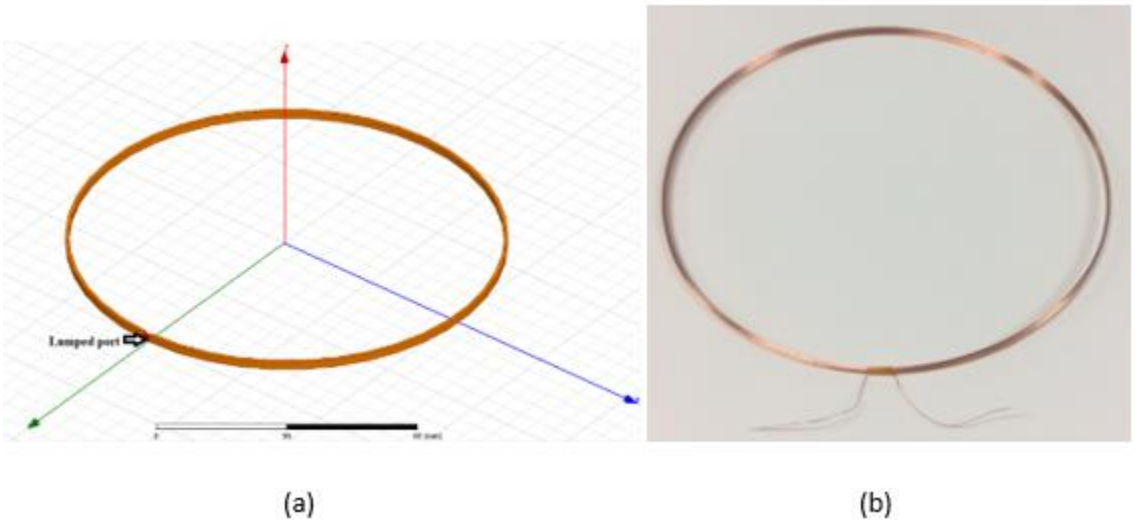

Fig. 4. The loop antenna coil: (a) the design model, (b) the implemented prototype

4.1.2 Isotropic metamaterial:

An isotropic metamaterial is an artificial material with specific electromagnetic properties such as electromagnetic band-gap structures (EBG). EBG materials are periodic structures that are composed of metal, dielectric or metallo-dielectric materials. These EBG structures can prevent EM wave propagation in spatial directions and at certain frequencies. Therefore, they can be used as spatial and frequency filters.

In antenna applications, there are various configurations of EBG structures which are classified into four main categories: photonic band-gap structure (PBG), defected ground structure (DGS), artificial magnetic conductor (AMC), high impedance electromagnetic surfaces (HIS). The specific propagation properties found in EBG structures are promising for several antenna applications, including miniaturization, coupling reduction, gain increase. In this thesis, a compact four arms spiral defected ground structure (SDGS) is designed to produce multi-electromagnetic band-gap and minimize the cross-polarization effect. This four-arm spiral geometry was proved by [11] to successfully eliminate the cross polarized fields.

In addition, it is also designed to back the loop antenna coil and enhance magnetic field intensity for a directional field distribution. In other words, a low profile directional loop antenna coil is designed to achieve a uniformly distributed and improved magnetic field.

The results in [11] show that the absorptivity of EM waves is about 100% near the resonant frequency of the isotropic metamaterials. Therefore, the metamaterials can be used as a narrow band absorber. The thickness of the metamaterials determines the width of the band. As the cross polarization affects the operating frequency and bandwidth proved by [12].

Therefore, in order to eliminate the cross-polarization effect, a four-arm spiral element is chosen as the shape of the unit element of the isotropic metamaterial. This geometry does not generate a cross polarization. In Fig.5., the four arms spiral shape is designed by using circuit marker pen manufactured by AgIC on a photo paper 105 mm x 105 mm with a silver ink.

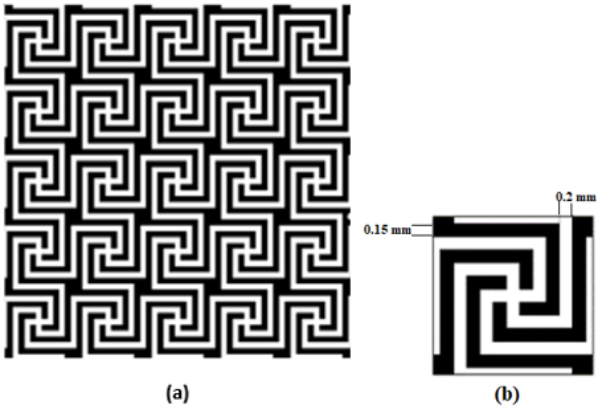

Fig. 5. Isotropic metamaterial: (a) unit element, (b) unit cell

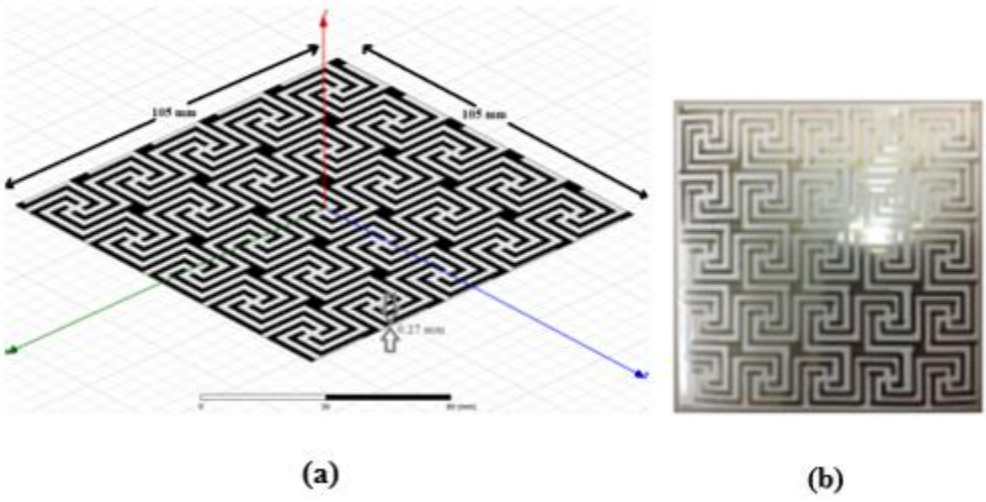

Fig. 6. Proposed isotropic metamaterial: (a) designed unit element, (b) prototyped unit element

4.1.3 Anisotropic metamaterial:

Since the bandwidth increases with the addition of the metamaterial layer number; the absorption is dependent on the polarization direction of the incident electromagnetic wave for the anisotropic metamaterials. Therefore, the role of the anisotropic metamaterial here is to be the polarization tunable absorber. The metamaterial layer number can also determine the frequency for the maximum absorption as for the multilayer system. An anisotropic metamaterial is manufactured by 3D printing as shown in Fig.7. by considering the

methodology of a uniaxial metamaterial proved by [17] in order to improve the working efficiency of the MMLPA antennas.

Fig. 7. Anisotropic metamaterial type 1: (a) unit element, (b) unit cell

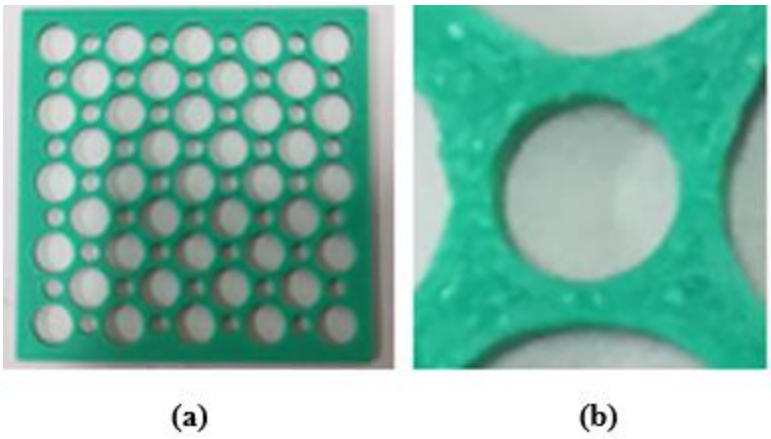

Fig. 8. Anisotropic metamaterial type 2: (a) unit element, (b) unit cell

4.2 Design procedure using a full-wave finite-element method

Low profile MMLPA systems are designed using loop antenna coils backed isotropic and anisotropic metamaterials. The loop antenna coil is placed 3 mm above the isotropic metamaterial layer, which is further backed by the anisotropic metamaterial layer placed 3.27 mm away, since the photo paper's thickness is 0.27 mm. This anisotropic metamaterial layer is then backed by a ground plane according to its thickness. As discussed above, two

kinds of anisotropic metamaterials are used in this thesis and each of them has two different thicknesses of this layer which are t_{am1} = 3 mm and t_{am2} = 5 mm. Consequently, four types of MMLPA system are designed and analyzed:

MMLPA-11: backed with anisotropic metamaterial type 1 and its thickness is t_{am1} = 3 mm;

MMLPA-21: backed with anisotropic metamaterial type 2 and its thickness is t_{am1} = 3 mm;

MMLPA-12: backed with anisotropic metamaterial type 1 and its thickness is t_{am2} = 5 mm;

MMLPA-22: backed with anisotropic metamaterial type 2 and its thickness is t_{am2} = 5 mm;

It is important to note that each of these antennas has the same specifications and geometries for the loop antenna coil, the isotropic metamaterial and the ground plane.

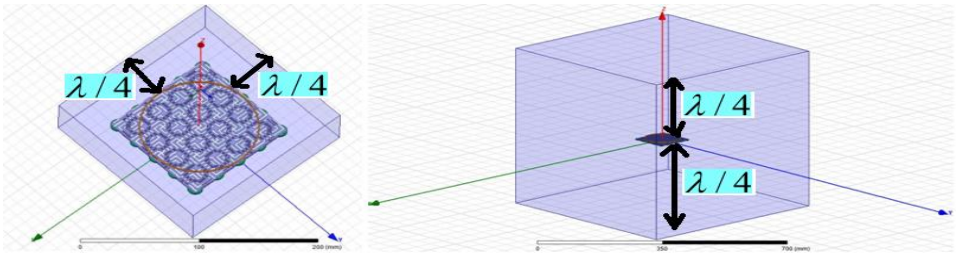

Fig. 9. Radiation boundaries structures of MMLPA-11: (a) Operating frequency 2.4 GHz ($\lambda = 12.5$ cm), (b) Operating frequency 315 MHz ($\lambda = 95.2$ cm)

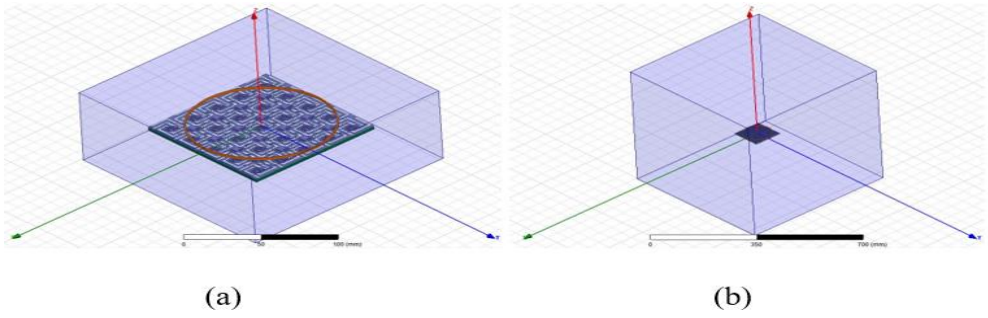

Fig. 10. Radiation boundaries of MMLPA-21: (a) at 2.4 GHz, (b) at 315 MHz

The realization of these metamaterials in our design procedure requires an infinite repetition of the unit element in the direction of the lattice vectors. This requirement is

achieved by imposing boundary conditions on the unit element as shown in Fig.9. and Fig.10. HFSS^{TM} v.15, which is a finite element method (FEM) based full wave simulator, is used to extract the S parameters. There are two methods in HFSS to extract the S parameters: either using perfect electric and perfect magnetic (PE-PM) boundary conditions or using master-slave boundary conditions. In the case of cubic-shaped unit element structure, these two methods are equally effective. However, the master-slave boundary conditions can also cover complex polygon-shaped structures. Therefore, in this thesis, master-slave boundary conditions method is chosen for the extraction of the S parameters. The boundary conditions at the master are enforced at the slave's surface in order to realize an infinite periodic repetition as shown in Fig. 11. and Fig. 12. below.

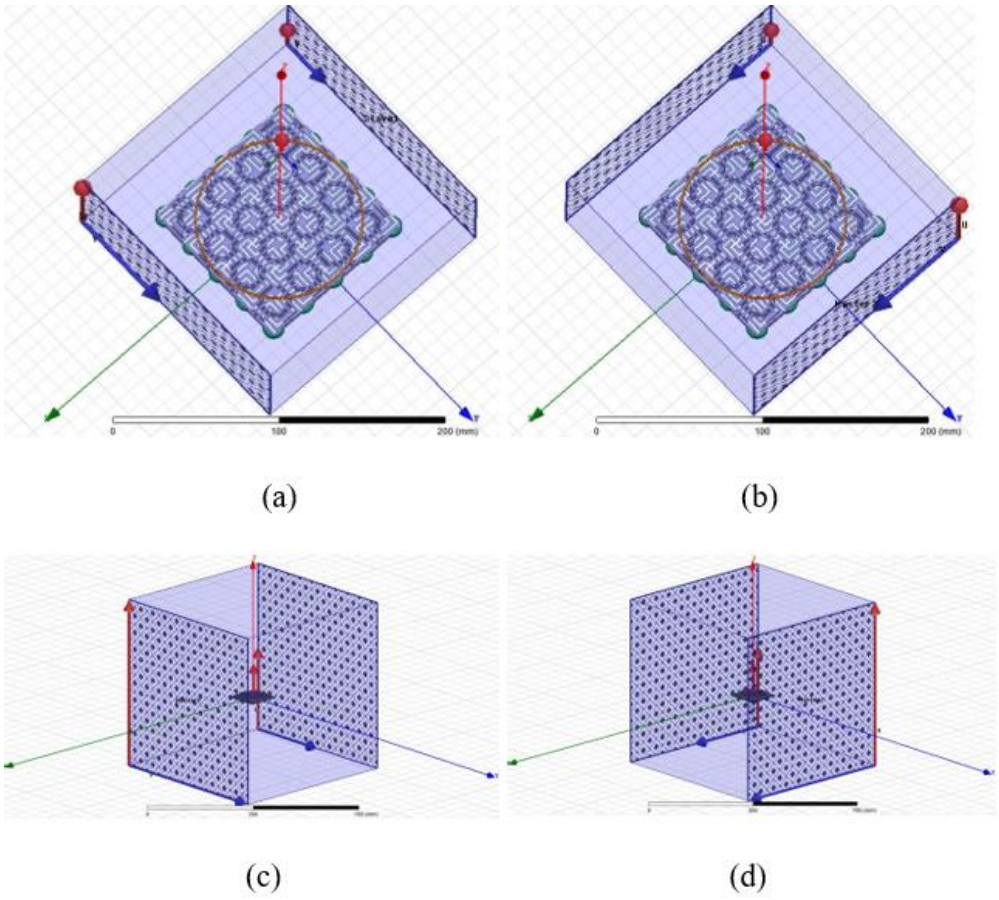

Fig. 11. Simulation model of MMLPA-11 with the master-slave boundary condition: (a) the first master-slave boundary pair at 2.4 GHz, (b) the second master-slave boundary pair at 2.4 GHz, (c) the first master-slave boundary pair at 315 MHz, (d) the second master-slave boundary pair at 315 MHz.

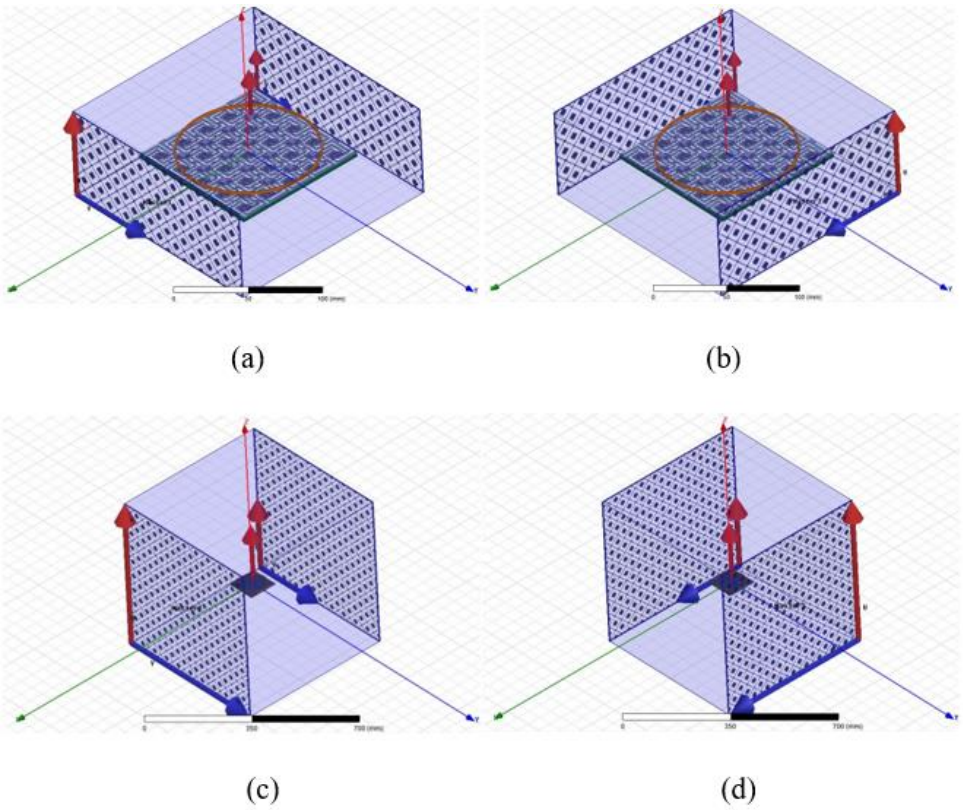

Fig. 12. Simulation model of MMLPA-21 with the master-slave boundary condition: (a) the first master-slave boundary pair at 2.4 GHz, (b) the second master-slave boundary pair at 2.4 GHz, (c) the first master-slave boundary pair at 315 MHz, (d) the second master-slave boundary pair at 315 MHz.

Once the boundary conditions are set, excitation ports are required to excite the structure. HFSS provides two options for the excitation: one using wave port, the second using floquet port as shown in Fig. 13 and Fig. 14. below.

On one hand, the wave port, which is equivalent to a semi-infinite waveguide, can excite the structure with the incident wave perpendicular to the surface of the port. On the other hand, the floquet port, which is important in situations where the direction of propagation of the incident wave is in the direction of the periodicity, can simulate obliquely incident waves. In this work, wave port cannot be applied since the plane perpendicular to the direction of propagation carries the periodic boundary conditions, and the floquet port is only option that can be used with the master-slave boundary conditions.

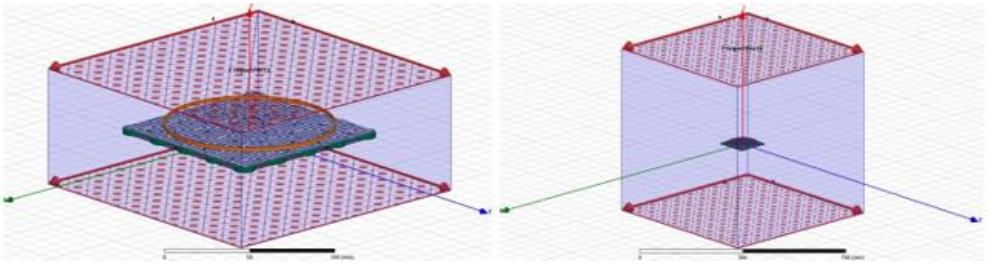

(a) (b)

Fig. 13. Unit element excitation of MMLPA-11: (a) Floquet port at 2.4 GHz, (b) Floquet port at 315 MHz

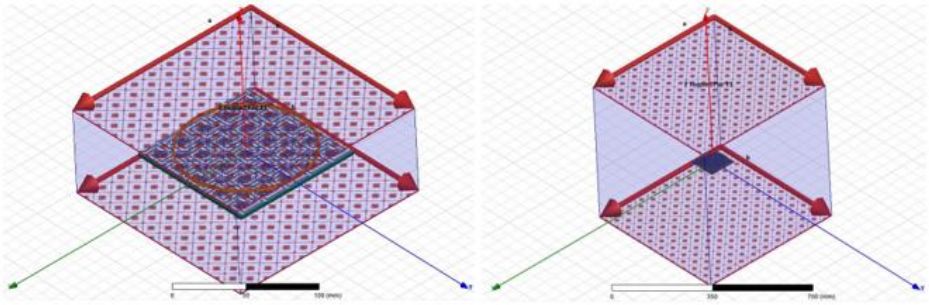

(a) (b)

Fig. 14. Unit element excitation of MMLPA-21: (a) Floquet port at 2.4 GHz, (b) Floquet port at 315 MHz

Similarly, we do the same method for the simulation design of antenna-12 and antenna-22 at these two frequencies.

Chapter 5

Simulation and experimental results

5.1 Simulation results

The following figures are the simulation results for the MMLPA-11 at 2.4 GHz using HFSS software. The scattering parameter S11 acts as return loss since the antenna is a one-port device. Fig. 15. shows the simulated return loss of MMLPA-11 equal to -24.5052 at resonant frequency 2.3997 GHz.

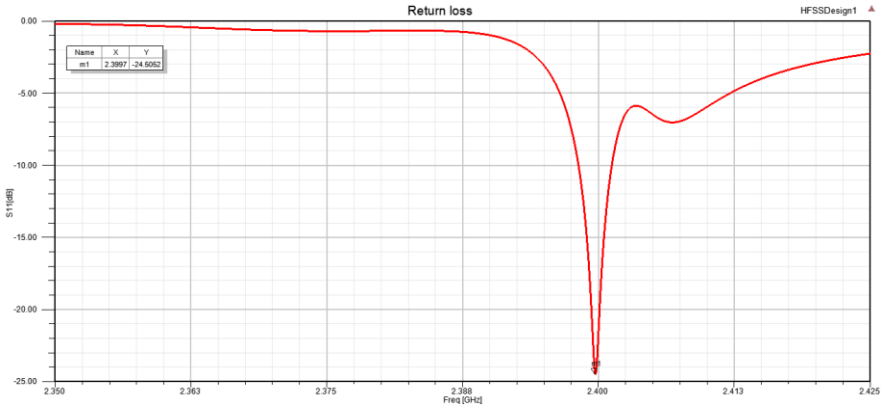

Fig. 15. MMLPA-11. Return loss at 2.4 GHz

In addition, the antenna is matched to the transmission line and more power is delivered to the antenna since the voltage standing wave ratio (VSWR) of MMLPA-11 is equal to 1.12, which is close to the ideal (VSWR = 1), at 2.4 GHz as shown in Fig. 16. below.

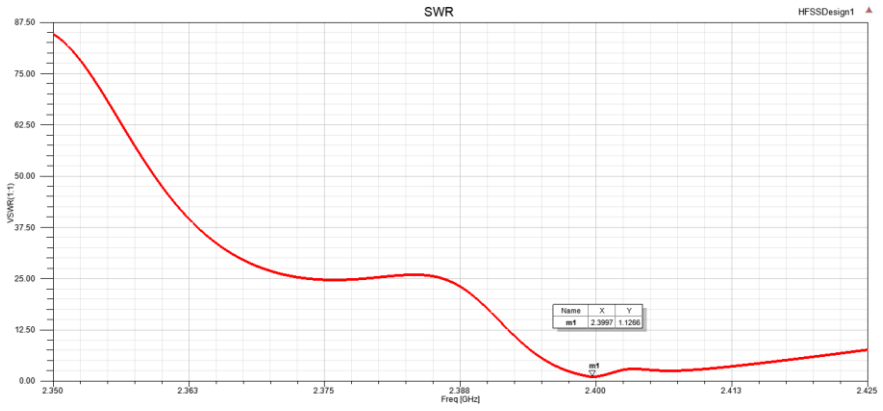

Fig. 16. MMLPA-11. VSWR at 2.4 GHz

A graphical presentation of signal distribution of the antenna is given by radiation pattern. The two-dimensional (2D) and three-dimensional (3D) radiation patterns for MMLPA-11 at 2.4 GHz are obtained as shown in Fig. 17. and Fig. 18. respectively.

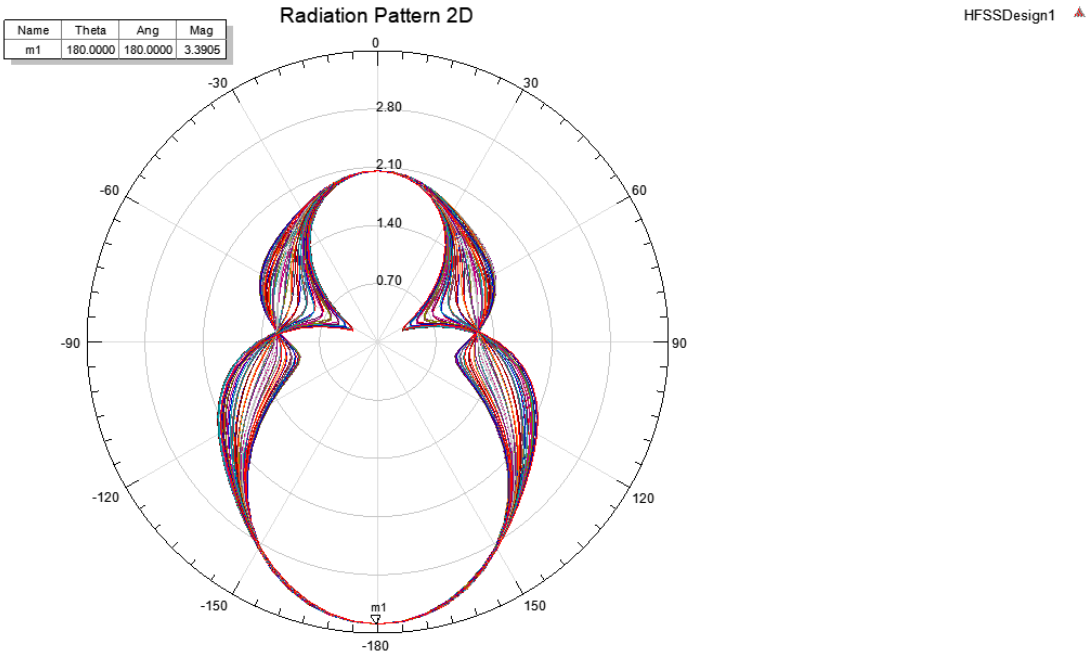

Fig. 17. MMLPA-11. Radiation pattern 2D at 2.4 GHz

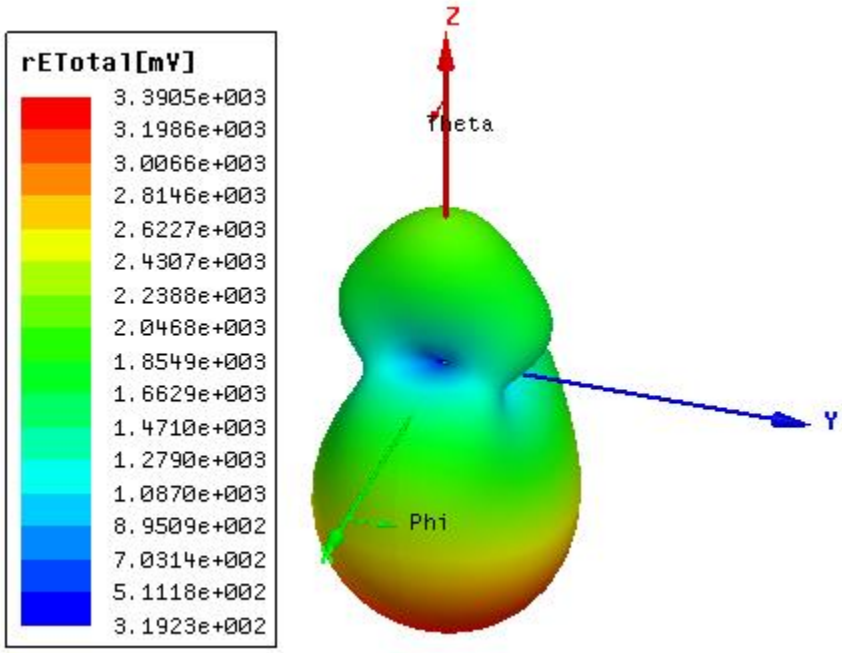

Fig. 18. MMLPA-11. Radiation pattern 3D at 2.4 GHz

The two- and three-dimensional directivity patterns of MMLPA-11 at 2.4 GHz are also represented in the Fig. 19. and Fig. 20. respectively.

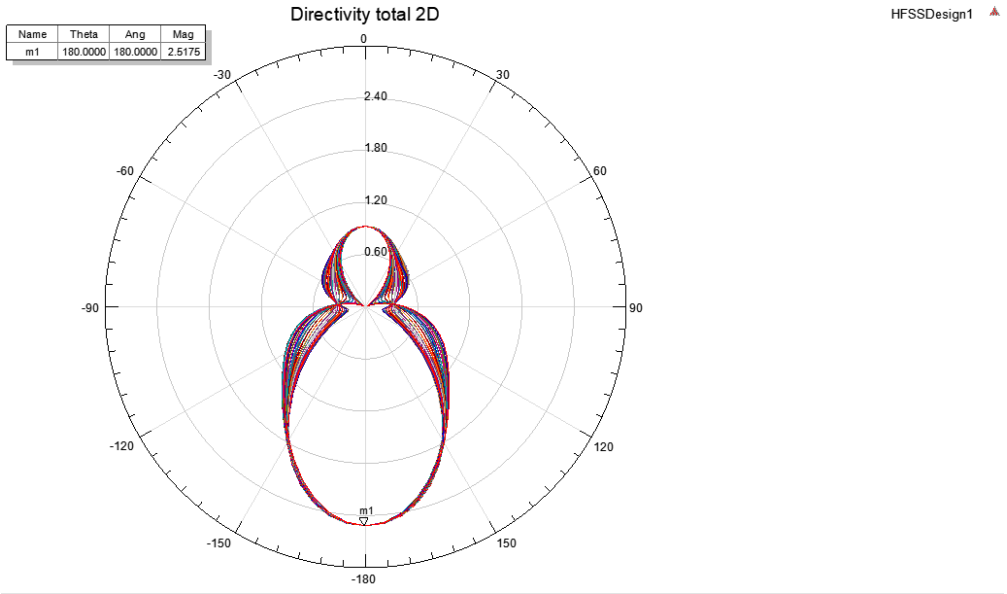

Fig. 19. MMLPA-11. Directivity total 2D at 2.4 GHz

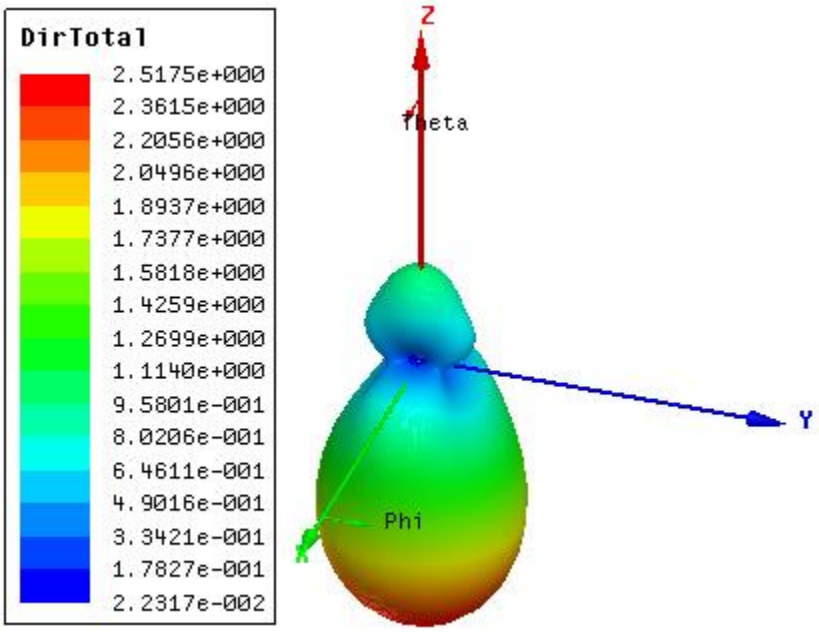

Fig. 20. MMLPA-11. Directivity total 3D at 2.4 GHz

The above figures show that MMLPA-11 has high directivity along z axis which is also the axis of the circular loop antenna. However, for a circular loop antenna without the metamaterial layers, the field radiated along its axis is zero [18].

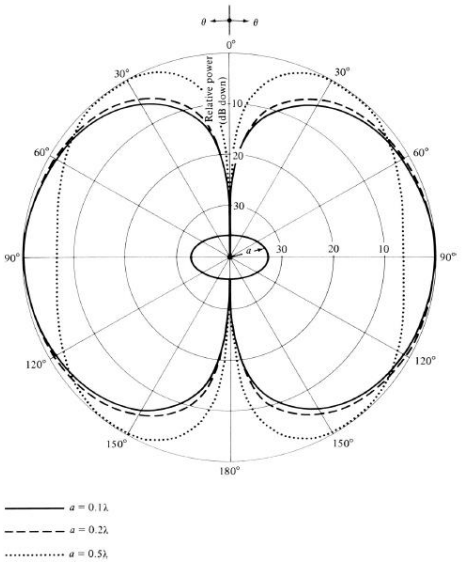

Fig. 21. The 2D radiation patterns for a circular loop antenna with radius $a = 0.1\lambda$, 0.2λ, and 0.5λ [18]

Therefore, these patterns indicate that the field radiated by the MMLPA-11 along xy plane which is perpendicular to the axis of the circular loop antenna coil is zero. In other words, the metamaterial layers enhance the magnetic field intensity in one directional field distribution.

A gain total of 2.29 dBi is obtained for the MMLPA-11 as shown in Fig. 22. Below.

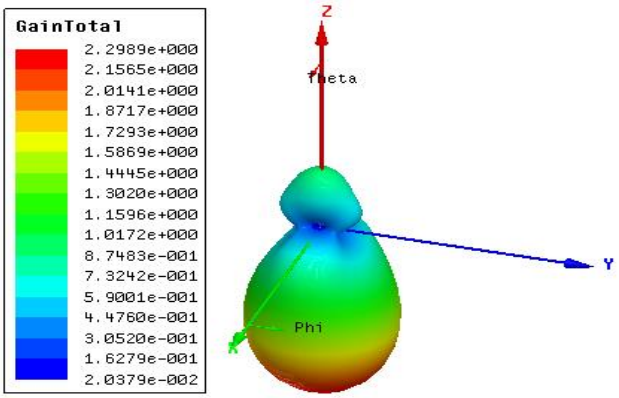

Fig. 22. MMLPA-11. Gain total at 2.4 GHz

It is important to note that it took time with very long computation process when performing the simulation of theses antennas in HFSS. Therefore, at the time of writing, we didn't get the simulation results for the remaining antennas yet. The analysis is supported by the measurement results.

5.2 Measurement results

The four prototyped MMLPA antennas are shown in Fig. 23. below.

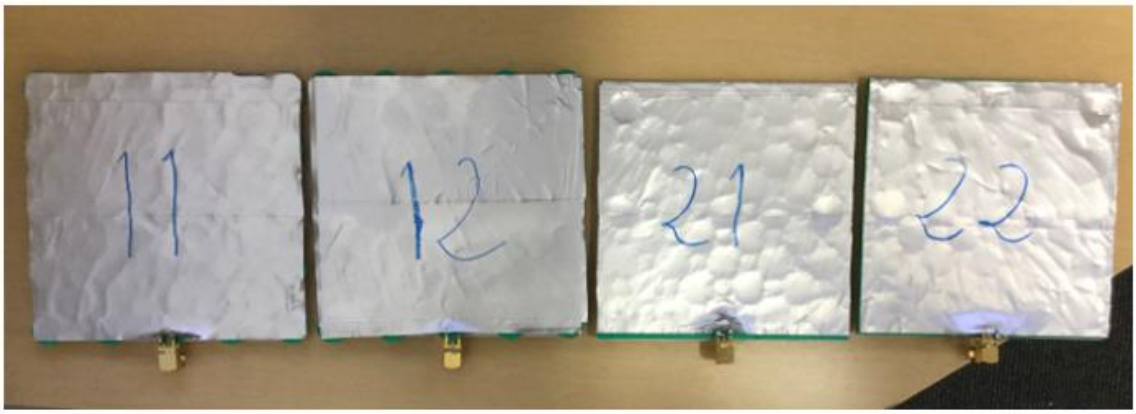

(a)

(b)

Fig. 23. The four prototyped MMLPA antennas

The following figures represent the measurement results of the return loss for all of the 4 MMLPA antennas at 2.4 GHz and at 315 MHz respectively.

Fig. 24. shows the return loss of MMLPA-11 at 2.4 GHz. We can notice that there is a good agreement compared with the related simulation result in Fig. 15.

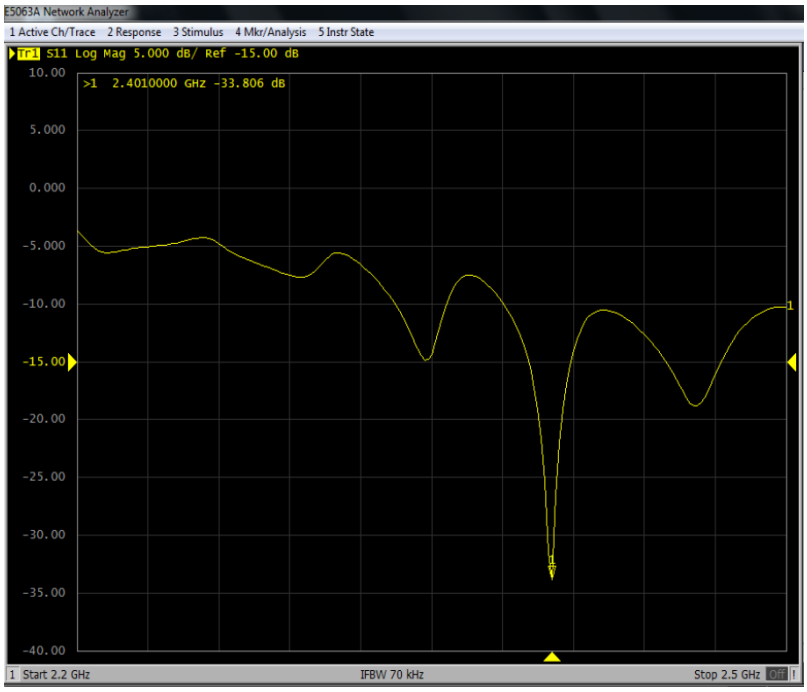

Fig. 24. MMLPA-11. Return loss at 2.4 GHz

At 315 MHz, the obtained return loss is -7.9357 dB as shown in Fig. 25. below.

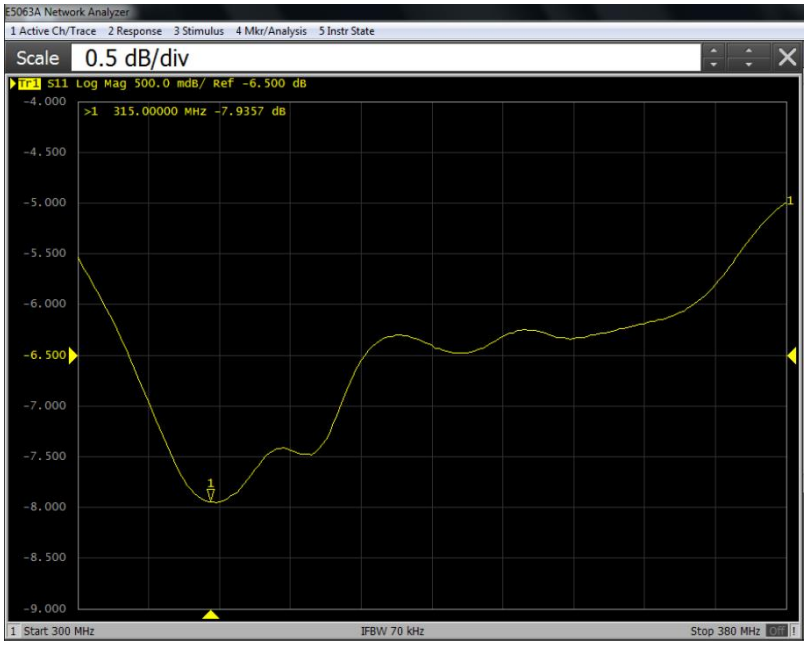

Fig. 25. MMLPA-11. Return loss at 315 MHz

For the MMLPA-12, the return loss at 2.4 GHz is -26.475 dB as shown in Fig. 26.

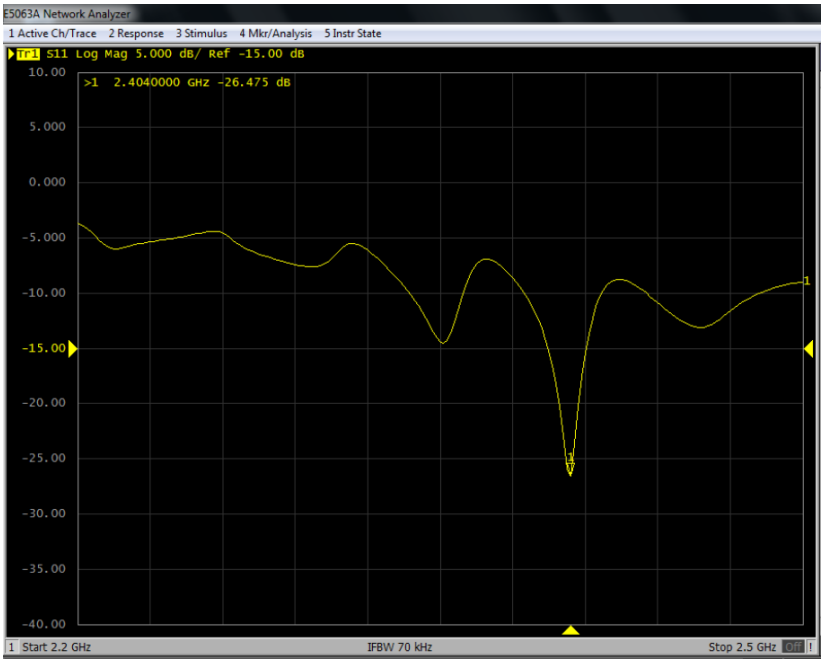

Fig. 26. MMLPA-12. Return loss at 2.4 GHz

However, at 315MHz, the resonant frequency shifts into 386 MHz with return loss -13.246 dB as shown in Fig.27. This is due to the increase of the thickness of the anisotropic metamaterial type 1.

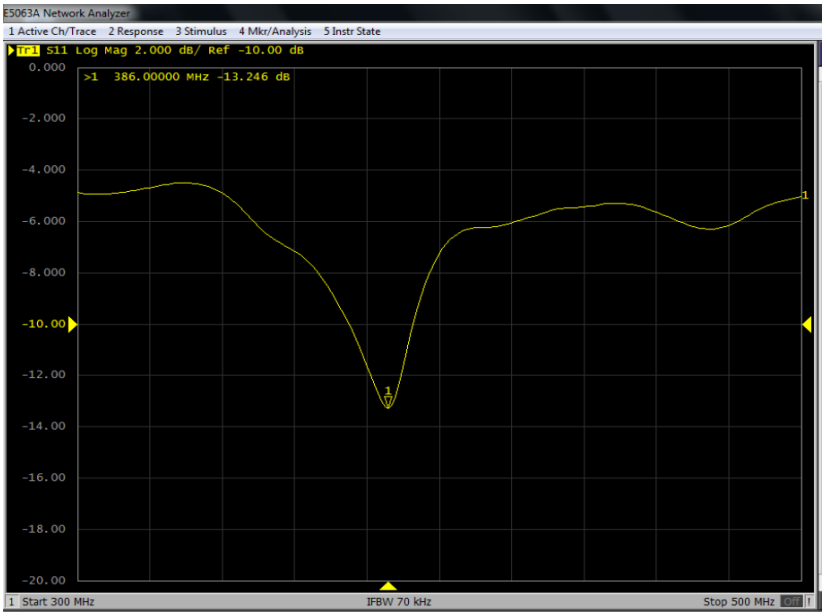

Fig. 27. MMLPA-12. Return loss at 315 MHz

In Fig.28. the return loss for MMLPA-21 at 2.4 GHz is -39.724 dB which is lower compared to the reflection coefficient of MMLPA-11 shown in Fig. 15.

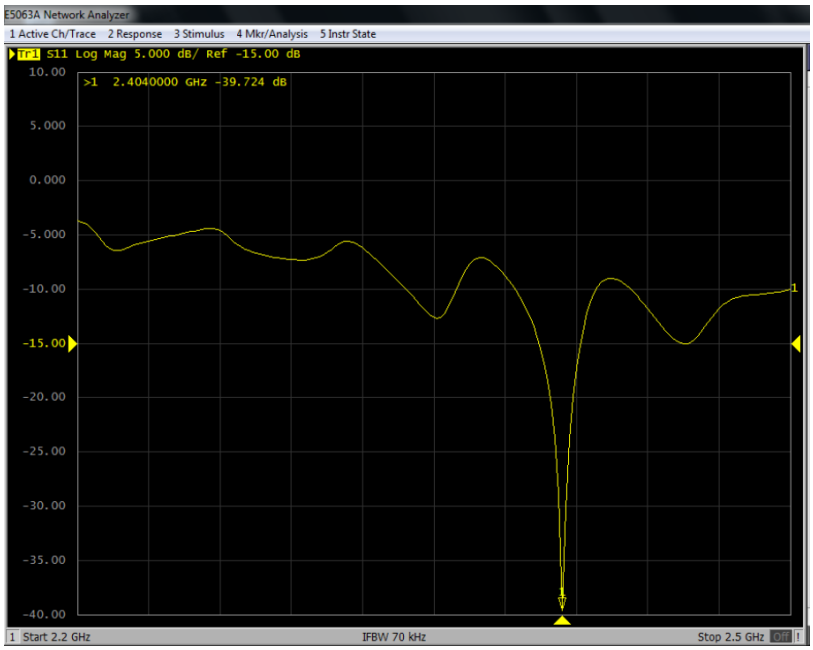

Fig. 28. MMLPA-21. Return loss at 2.4 GHz

However, from the Fig. 29. below, there is no resonant frequency between the frequency range from 300MHz to 380 MHz for this MMLPA-21 antenna.

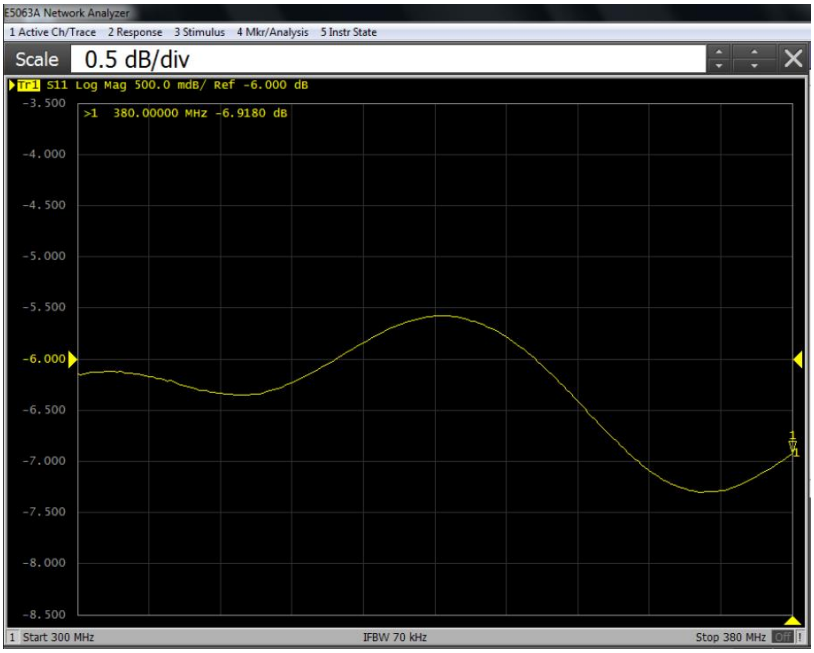

Fig. 29. MMLPA-21. Return loss at 315 MHz

Finally, in Fig. 30., the return loss at 2.4 GHz of MMLPA-22 is -36.545 dB which is also lower compared to the reflection coefficient of MMLPA-11 shown in Fig. 15.

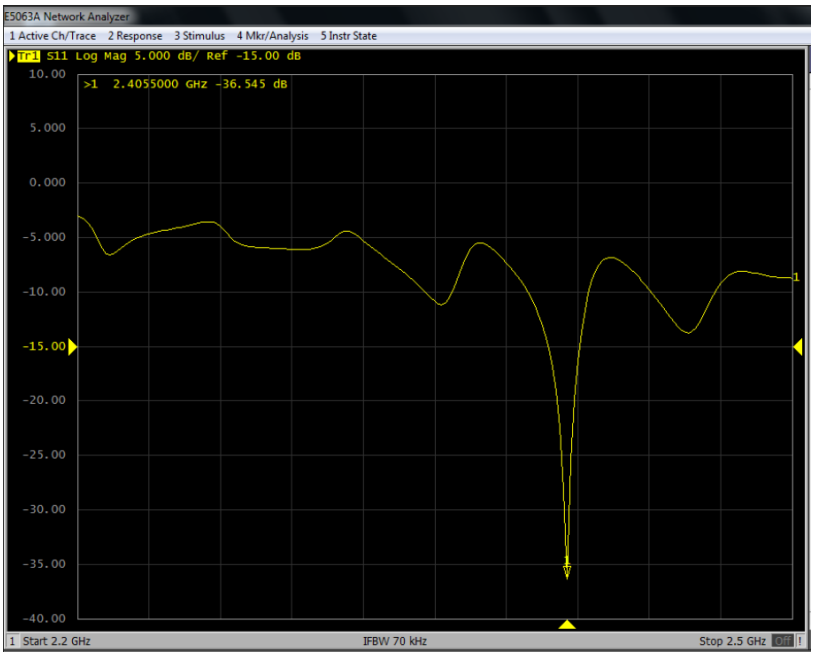

Fig. 30. MMLPA-22. Return loss at 2.4 GHz

However, from the Fig. 31. below, there is no resonant frequency between the frequency range from 300MHz to 380 MHz for this MMLPA-21 antenna.

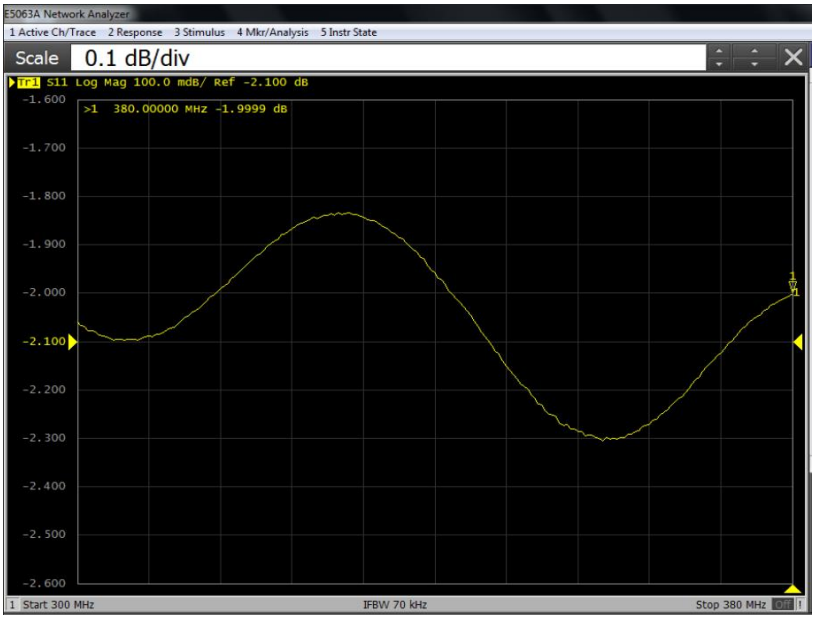

Fig. 31. MMLPA-22. Return loss at 315 MHz

5.3 Study of the effect of metal presence in the vicinity of the MMLPA transceivers

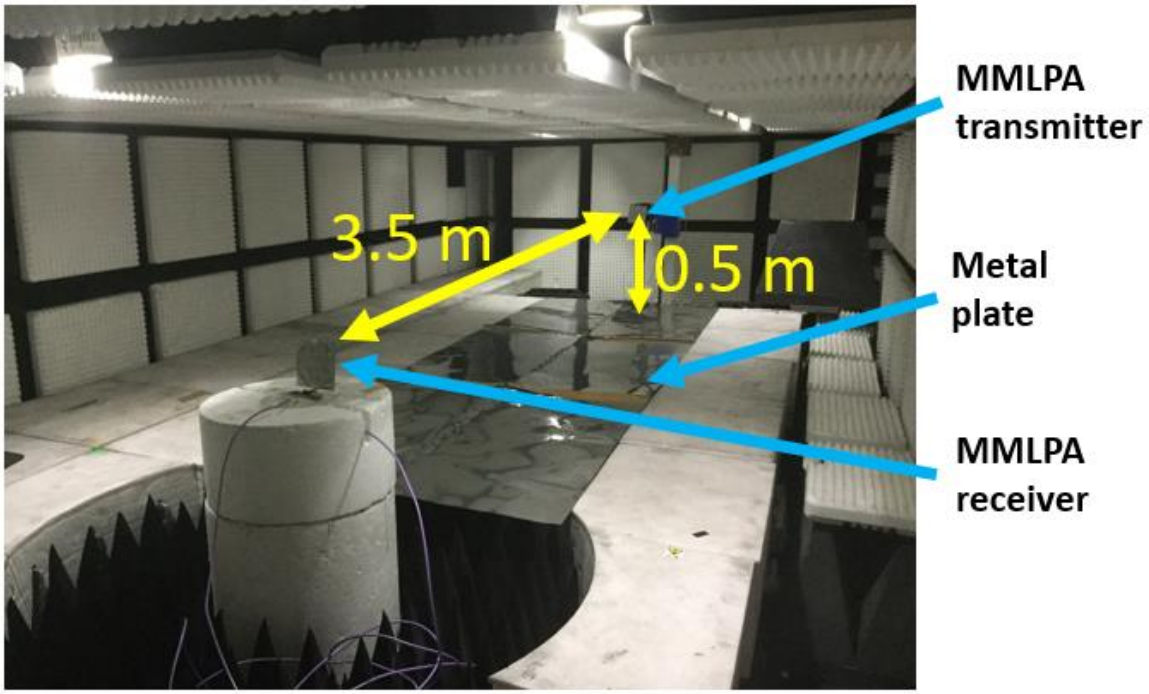

Fig. 32. Experiment setup inside an anechoic chamber testing the effect of metal presence in the vicinity of the MMLPA system

In this experiment setup, MMLPA-11 and MMLPA-21 are utilized as transmitters while MMLPA-12 and MMLPA-22 are the receivers, respectively.

The communication range is set at 3.5 m and the experiment is performed inside an anechoic chamber. The aim of the measurement is to study the effect of metal presence in the vicinity of MMLPA transceivers.

In this work, a metal plate 1 m x 3 m made by steel is placed in between the transmitter antenna (Tx) and the receiver antenna (Rx) as shown in Fig. 32. The height is 0.5 m from the surface of the metal plate to the axis of the antennas. The following figures indicate the effect of the presence of this metal plate for those MMLPA antennas.

In Fig. 33. and Fig. 34. below, MMLPA-11 is the transmitter while MMLPA-12 is the receiver. It shows that the presence of the metal plate increases the received power from -62.22 dBm to -58 dBm.

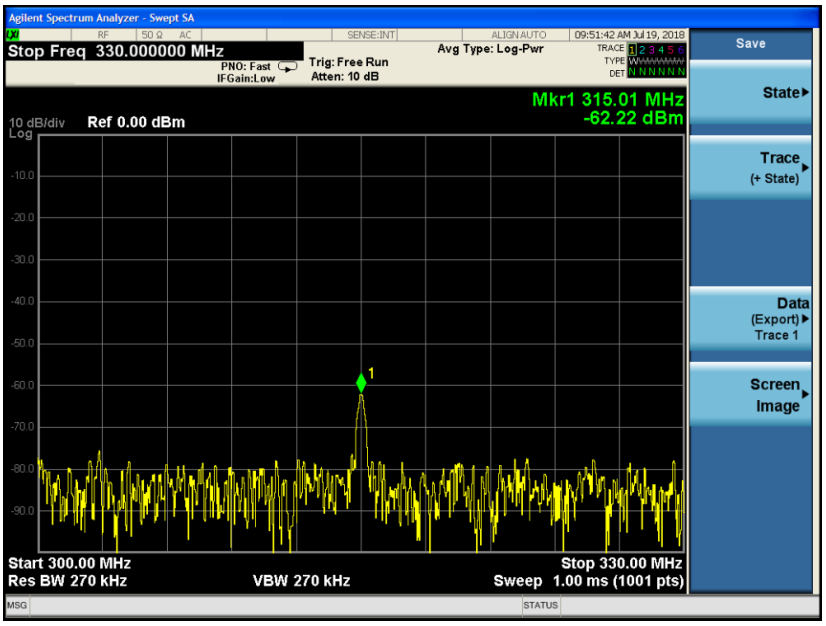

Fig. 33. Tx: MMLPA-11, Rx: MMLPA-12, without the metal plate

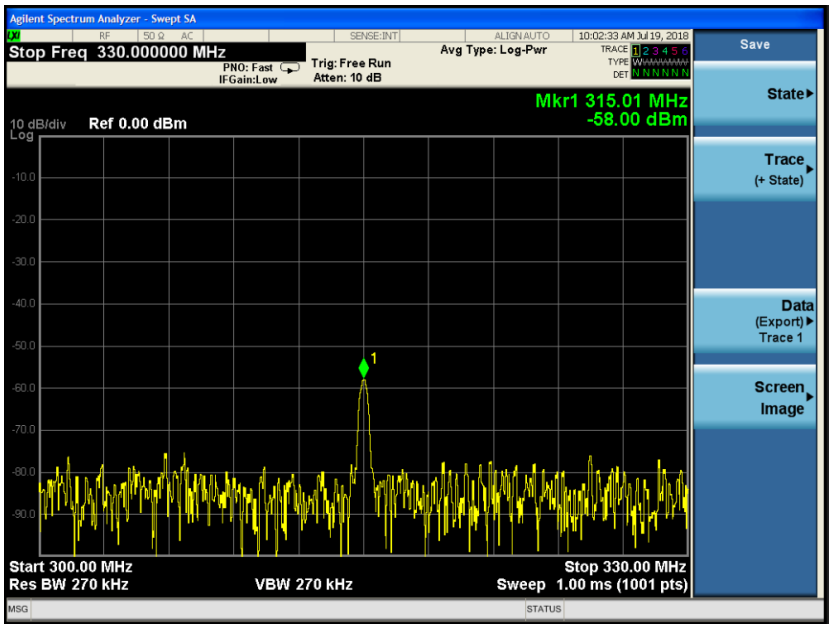

Fig. 34. Tx: MMLPA-11, Rx: MMLPA-12, with the metal plate

In Fig. 35. and Fig. 36., MMLPA-21 is the transmitter while MMLPA-22 is the receiver. It also shows that the presence of the metal plate increases the received power from -75.45 dBm to -68.77 dBm.

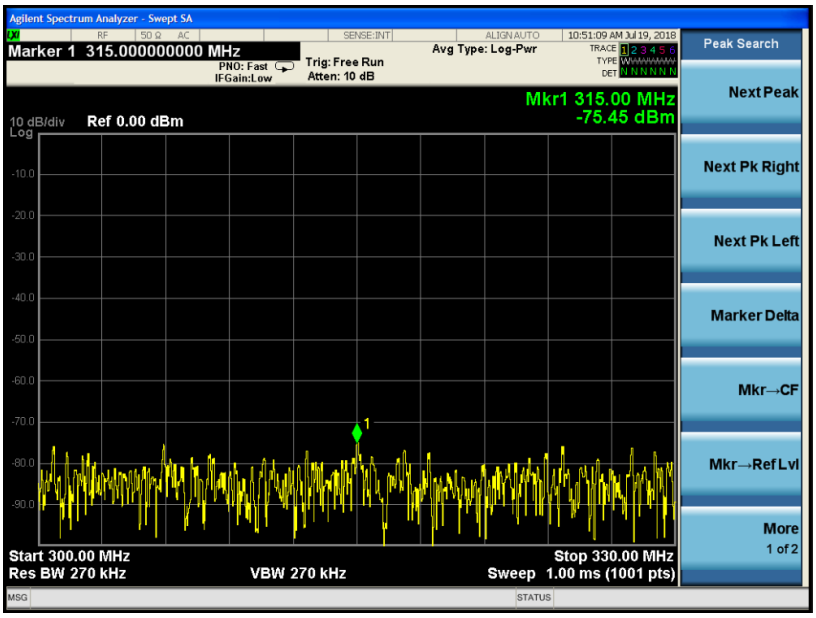

Fig. 35. Tx: MMLPA-21, Rx: MMLPA-22, without the metal plate

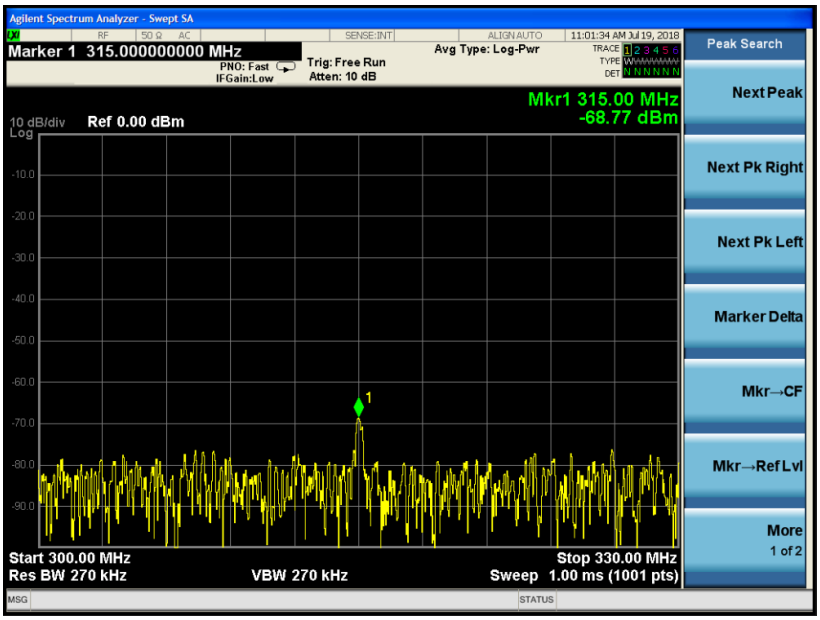

Fig. 36. Tx: MMLPA-21, Rx: MMLPA-22, with the metal plate

Chapter 6

IoT application

6.1 System setup

The system setup presented in Fig. 37. below is developed for the MMLPA-IoT application.

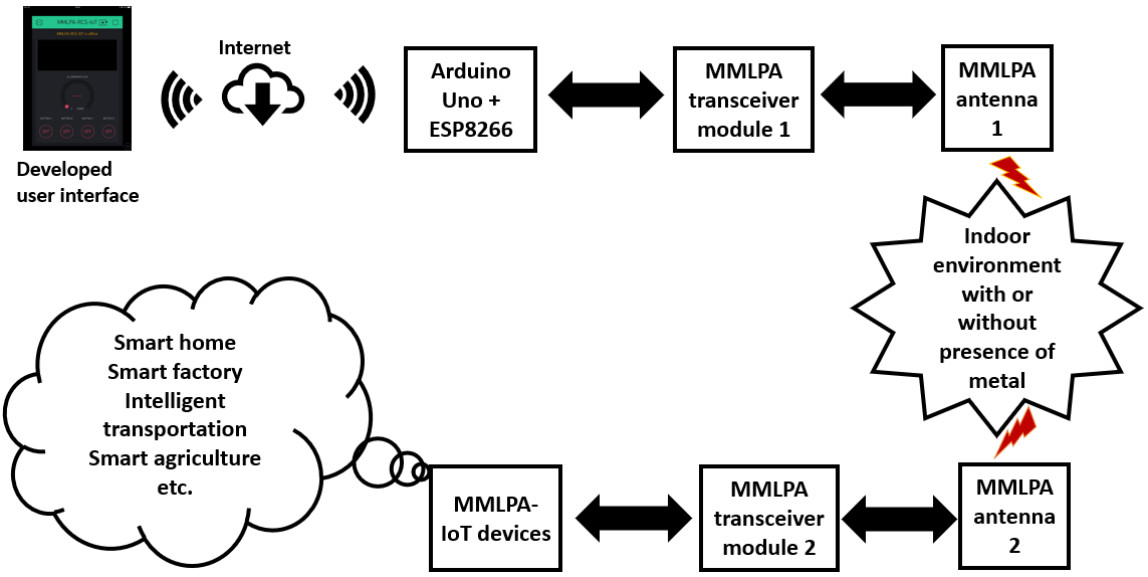

Fig. 37. MMLPA-IoT application system setup

In this system, we send order from smartphone to MMLPA-IoT devices like power outlet sockets, lamps, home appliances, etc.

On one hand, the smartphone is connected to the Internet while a WiFi module composed with Arduino Uno and ESP8266 is also connected to the Internet via the wireless local area network (WLAN). In this work, we utilized the local WiFi of our laboratory. Then, this module is connected to MMLPA transceiver module 1 including MMLPA antenna 1 which is one of our MMLPA antennas. We assume that the transmission medium is air with or without presence of metal in the vicinity of the transceiver antennas. All those modules are considered as part of the control unit.

On the other hand, the MMLPA-IoT device is composed with MMLPA transceiver module 2 including MMLPA antenna 2 which is also one of our MMLPA antennas.

6.2 MMLPA-RCS-IoT

Here RCS stands for Remote Control Switch. Therefore, the aim of this application is to control electrical switches remotely via our smartphone using Internet connection. Fig. 38. shows the graphical user interface on the smartphone, in this work we use instead iPad. The control menu is composed with four button widgets, a gauge widget and a widget display. The four button widgets are utilized to control a switch remotely with four channels using our MMLPA system. The gauge widget is used for hardware feedback while the widget display is for software feedback. In this thesis, we control the lights remotely, that is why our hardware feedback will measure the illuminance in Lux. The widget display will display the name of the button which was activated only if the order sent by the iPad was received by the MMLPA-IoT device. Every time we push a given button on the iPad, the order is sent through the Internet to the MMLPA-IoT device, which sent the corresponding code through radio waves to the remote device using our MMLPA-antennas.

Fig. 38. Developed User Interface on iPad for remote control switch with four channels using our MMLPA system

Chapter 7

Conclusion and Future Work

It has been shown that our Multilayered Metamaterials Low Profile Antenna using Magnetic Induction communication scheme can improve the directivity of a loop antenna coil and its efficiency. Four prototypes of MMLPA system have been realized and measured where good agreement is achieved between simulation and measurement results. The magnetic field intensity is enhanced in one directional field distribution as expected. An IoT application was developed. In this thesis, it has been proved that the presence of metal in the vicinity of the MMLPA system can increase the received power as well. Therefore, this novel communication system can be applied for IoT devices working on the 2.4 GHz and 315 MHz band. Since the antennas are low profile, they can be mounted to buildings' wall, cars, etc. So, they are suitable for connecting IoT devices in indoor environment even with the presence of metal structure in the vicinity of the antennas.

Further improvements to the technique should allow a full study of the effect of the communication media especially when operating at lower frequency band.

Appendix

It is important to note that before printing our anisotropic metamaterial, we need to prepare a stl file for the desired 3D geometry that can be read by the 3D printer. In this work, in order to build stl file, we have utilized OpenSCAD which is a free software application for creating solid 3D CAD objects via script-only based modeler.

A.1. Development of the 3D geometry of the anisotropic metamaterial type 1

```
//Design of the internal cylinders, file name after rendering: AnisotropicMetamaterial1-Part1.stl

// diameter

start = 6.4;

incr = 0;

// distance of one cylinder to the next

dx = 24;

for(x=[1:4])

for(y=[1:4])

   translate([x*dx,y*dx,0])

   cylinder(h = 3, r = start+x*incr+y*incr, $fs=0.5);


//Design of the remaining geometries, file name after rendering: AnisotropicMetamaterial1-Part2.stl

// Model parameters

model_filename = "AnisotropicMetamaterial1-Part1.stl";

model_scale = .7;                                   // Scale factor for the model
```

```
model_translate = [0,0,0];              // Translate model relative to mold

model_rotate = [0,0,0];                 // Rotate model relative to mold


// Mold parameters

mold_width = 24;            // Width of the mold

mold_height = 24;           // Height of the mold


// metamaterial parameters

metamaterial_thickness = 1.5;       // Thickness of all metamaterials

metamaterial_height = 3;            // Height of the metamaterials

metamaterials = true;               // metamaterials or no metamaterials


// Removable metamaterial parameters

removable_metamaterial = false;                 // Do we want one metamaterial to be removable?

removable_metamaterial_thickness = 1;           // Thickness of the removable metamaterial

wiggle_room = 0.25;                 // Fit between metamaterial and slot


// Base parameters

base_height = 0;            // Thickness of the base

grid_cylinder();
```

```
dx = 24;
for(x=[0:3])
for(y=[0:3])
   translate([x*dx,y*dx,0])
   generate_mold();

module grid_cylinder() {
// diameter
start = 6.4;
incr = 0;

// distance of one hole to the next
dx = 24;
union(){
   for(x=[0:4])
   for(y=[0:4])
      translate([x*dx,y*dx,0])
      cylinder(h = 3, r = start+x*incr+y*incr, $fs=0.5);
   }
}
```

```
module generate_mold() {
        difference() {
                union() {
                        difference() {
                                // metamaterials and base
                                translate(v = [12,12,metamaterial_height/2 + base_height/2])
                                        cube(size = [mold_width,mold_height,metamaterial_height+base_height], center = true);

                                // Hollow out the mold, leaving metamaterials and a base
                                translate(v = [12,12,25 + base_height])
                                        if(metamaterials)
                                                cube(size = [mold_width - metamaterial_thickness*2, mold_height - metamaterial_thickness*2, 50], center = true);
                                        else
                                                cube(size = [mold_width, mold_height, 50], center = true);
                        }

                        // Scale, translate and import an external STL
                scale(v = [model_scale, model_scale, model_scale])
                   translate(model_translate)
```

```
        rotate(model_rotate)
            import(model_filename);
        }

        // Create slot for removable metamaterial
        if(removable_metamaterial) {
            // Remove the old metamaterial
            translate(v = [mold_width/2 - metamaterial_thickness/2, 0, base_height + 25])
                cube(size = [metamaterial_thickness, mold_height - metamaterial_thickness*2, 50], center = true);

            // Create a notch for the removable metamaterial
            translate(v = [mold_width/2 - metamaterial_thickness, 0, base_height + 25])
                cube(size = [removable_metamaterial_thickness + wiggle_room*2, mold_height - metamaterial_thickness + wiggle_room*2, 50], center = true);
        }

        // Remove any geometry popping out from under the mold
        translate(v = [0,0,-50])
            cube(size = [mold_width, mold_height, 100], center = true);
    }
```

```
    // Add removable metamaterial
    if(removable_metamaterial)
        translate(v = [mold_width/2 + 5, 0, metamaterial_height/2])
            cube(size = [removable_metamaterial_thickness, mold_height - metamaterial_thickness, metamaterial_height], center = true);
}
```

A.2. Development of the 3D geometry of the anisotropic metamaterial type 2

```
// diameter of the cylinders, file name after rendering: AnisotropicMetamaterial2.stl
start = 6.4;
incr = 0;
// distance of one hole to the next
dx = 21;
difference()
{
    translate([-dx,-dx,0]) cube([5*dx,5*dx,3]);
union()
{
for(x=[-0.5:3.5])
for(y=[-0.5:3.5]){
    translate([x*dx,y*dx,0])
    cylinder(h = 3, r = start+x*incr+y*incr, $fs=0.5);
```

```
    }
    union(){
    start = 6.4;
    incr = 0;
    dx = 21;
    for(x=[0:3])
    for(y=[0:3]){
        translate([x*dx,y*dx,0])
        cylinder(h = 3, r = start+x*incr+y*incr, $fs=0.5);
    }
    union(){
    start = 3.2;
    incr = 0;
    dx = 10.5;
    for(x=[-1:7])
    for(y=[-1:7]){
        translate([x*dx,y*dx,0])
        cylinder(h = 3, r = start+x*incr+y*incr, $fs=0.5);
    }
}
}
}
}
```

References

[1] R. Kranenburg and A. Bassi, “IoT challenges,” Com.. Mob. Comp., vol.1, no.1, pp.1-5, 2012.

[2] T. Liu and D. Lu, “The application and development of IoT,” in Proc. Int. Symp. Inf. Technol. Med. Educ. (ITME), 2012, vol. 2, pp. 991-994.

[3] I. F. Akyildiz and E. P. Stuntebeck, “Wireless underground sensor networks: Research challenges,” Ad Hoc Networks Journal (Elsevier), July 2006, vol. 4, pp. 669-686.

[4] J. B. Gulbhar, “A communication theoritical modeling and analysis of underwater magneto-inductive wireless channels,” IEEE Trans. on Wireless Com., 2012, vol. 11, no. 9, pp. 3326-3334.

[5] Z. Sun and I. F. Akyildiz, “Magnetic Induction communications for wireless underground sensor networks,” IEEE Trans. on Antenna and Propagation, July 2010, vol. 58, no. 7, pp. 2426-243.

[6] E. Shamonina, V. A. Kalinin, K. H. Ringhofer, and L. Solymar, “Magneto-inductive waveguide,” Electronics Letters, 2002, vol. 38, no. 8, pp. 371-373.

[7] H. Guo, “M2I: Channel modeling for metamaterial enchanced magnetic induction communications,” Antenna and propagation, IEEE transactions, 2015, vol. 63, no.11, pp. 5072-5087.

[8] N. Lopez, “Compact metamaterial antenna array for long term evolution (LTE) handset application,” IEEE International workshop on antenna, 2009, Santa Monica, CA, March 2009, pp. 1-4.

[9] B. Wang, W. Yerazunis, and K. H. Teo, “Wireless power transfer: metamaterials and array of coupled resonators,” Proceedings of the IEEE, 2013, vol. 101, no. 6, pp. 1359-1368.

[10] K. E. Hjelmstad and W. H. Pomroy, “Ultra low frequency electromagnetic fire alarm system for underground mines,” U.S. Dept. of the Interior, Bureau of Mines. Tech. Rep. 9377, 1991.

[11] D. M. Elsheakh and E. A. Abdallah, “Different Feeding Techniques of Microstrip Patch Antennas with Spiral Defected Ground Structure for Size Reduction and Ultra-Wide Band Operation,” Journal of Electromagnetic Analysis and Applications, Vol. 4, No. 1, 2012, pp.410-418.

[12] Dong Yunxia, “Electromagnetic Wave Absorber with Isotropic and Anisotropic Metamaterials”, International Journal of Materials Science. Vol. 6, No. 6, 2017, pp. 302-308.

[13] Y. Urzhumov and D. R. Smith, “Metamaterial enhanced magnetic Antenna coupling between magnetic dipoles for efficient wireless power transfer,” Physical Review B, 2011, vol. 83, no. 20, p. 205114.

[14] Zhi Ning Chen, “Review of Zero-Phase-Shift-Line Loop Antennas for UHF Near-Field RFID Readers” IEEE journal of radio frequency identification, vol. 1, no. 4,

December 2017.

[15] X. Chen, T. M Grzegorczyk, B. Wu, J. Pacheco, A. Kong, “Robust Method to retrieve the constitutive effective parameters of metamaterials,” Physics Review E, 70, July 2004, 016608.

[16] S. Arslanagic, T. V. Hansen, “A review of the scattering parameter extraction method with clarification of ambiguity issues in relation to metamaterial homogenization,” IEEE Antennas and Propagation Magazine, 55, 2, April 2013, pp. 91-106.

[17] Garcia, C. Roman, "3D printed spatially variant anisotropic metamaterials" (2014). ETD Collection for University of Texas, El Paso. AAI10118141.

[18] C. A. Balanis, “Antenna theory: analysis and design”, John Wiley & Sons, 2005.

Research Achievement

1. Tojoarisoa Rakotoaritina, Megumi Saito, Zhenni Pan, Jiang Liu, and Shigeru Shimamoto, “Multilayered Metamaterial Low Profile Antenna for IoT Applications”, in Proceedings of the 37th JSST Annual International Conference on Simulation Technology, OS7: IoT, D2D, V2X, and Wireless Communications towards Beyond 5G, Muroran Institute of Technology, Muroran City, Hokkaido, Japan, September 2018.